

## Synchronization mechanism and Arnold tongues for dust density waves

W. D. Suranga Ruhunusiri\* and J. Goree

*Department of Physics and Astronomy, The University of Iowa, Iowa City, Iowa 52242 USA*

(Received 1 November 2011; revised manuscript received 16 February 2012; published 2 April 2012)

The nonlinear phenomenon of synchronization is characterized experimentally for dust density waves, i.e., dust acoustic waves, which are self-excited due to an ion streaming instability. The waves propagate in a dust cloud with a natural frequency of 22 Hz. We synchronize these waves to a different frequency using a driving electrode that sinusoidally modulates the ion density. We study four synchronized states, with frequencies that are multiples of 1, 2, 3, and 1/2 of the driving frequency. Comparing to phenomena that are typical of the van der Pol paradigm, we find that synchronization of our waves exhibit the signature of the suppression mechanism but not that of the phaselocking mechanism. Additionally, synchronization of our waves exhibits three characteristics that differ from the van der Pol paradigm: a threshold amplitude that can be seen in the Arnold tongue diagram, a branching of the 1:1 harmonic tongue at its lower extremity, and a nonharmonic state. The latter state appears to be a nonlinear oscillation; it is neither at the natural frequency nor a synchronized state.

DOI: [10.1103/PhysRevE.85.046401](https://doi.org/10.1103/PhysRevE.85.046401)

PACS number(s): 52.27.Lw, 05.45.Xt, 52.35.Mw

### I. INTRODUCTION

A dusty plasma is a four-component plasma of electrons, ions, neutral gas atoms, and micron-size particles of solid matter. Dusty plasmas are found in nature, for example, in planetary rings, comet tails, interstellar clouds, and Earth's ionosphere [1–8]. In a laboratory, dusty plasma can be produced by introducing dust particles, i.e., small particles of solid matter, into a glow discharge plasma [7,9]. The dust particles are much more massive than the electrons, ions, or neutrals. In a laboratory experiment, the dust particles gain a negative electric charge by absorbing more electrons than ions. At sufficiently high dust particle concentrations, the dust particle can deplete electrons [10].

A collection of dust particles can sustain different kinds of waves [3,7,8]. The dust acoustic or dust density wave is a compressional mode that is analogous to the ion acoustic wave [11]. The concentration of dust particles is modulated, and due to their large mass the wave has a low frequency, which in laboratory experiments is typically 10–100 Hz [12]. At such a low frequency, this wave can be observed by video imaging [13]. Dust density waves can appear spontaneously, without any external excitation, as has been observed in the laboratory [14–43] and under microgravity conditions [44–47].

Dust density waves appear spontaneously because they are self-excited by an instability that is driven by streaming ions, similar to a Buneman-type instability in plasma [48–50]. The waves usually propagate parallel to the ion streaming direction. Such a streaming of ions is common in glow discharge plasmas, where it is driven by an ambipolar electric field. The ion-driven instability must compete with wave damping due to frictional drag of the dust particles as they move through the neutral gas [50] (and possibly Landau damping [51] and damping resulting from charge fluctuations [51–53]). At a sufficiently low gas density, damping is so weak that it cannot overcome the instability, and the self-excited dust density waves can grow to large amplitudes and become nonlinear [43].

Nonlinear phenomena for these waves have been observed experimentally, including harmonic generation [43], shocks [37], wave breaking [36], frequency clustering [47], and synchronization [30,38,39,46,54]. In theoretical models of the wave, the nonlinearities can arise in the convective derivative term of the dust momentum equation or in the electron density due to either the nonlinearity of the Boltzmann factor or due to depletion of electrons.

The nonlinear phenomenon we will investigate in this paper is synchronization, in which a self-excited oscillation or wave interacts with a driving force, resulting in an adjustment of the oscillation or wave frequency [55,56]. Synchronization was observed by Huygens for two pendulum clocks that were mechanically coupled [55]. Since then, synchronization has been observed in biological, chemical, electrical, and mechanical oscillatory systems [55,56].

Plasma physics experimenters have observed several kinds of waves and oscillations that exhibit synchronization. These include ion sound waves [57], ionization waves [58,59], drift waves [60–65], ion cyclotron waves [66], plasma relaxation oscillations [67–71], and beam plasma oscillations [72–74].

A common mathematical model that exhibits synchronization is a periodically forced van der Pol oscillator [75],

$$\ddot{x} - (\alpha - \beta x^2)\dot{x} + \omega_0^2 x = A_{\text{dr}} \cos(2\pi f_{\text{dr}} t), \quad (1)$$

which describes the position  $x$  of a harmonic oscillator with a natural frequency  $\omega_0 = 2\pi f_0$ , with terms for a nonlinear damping  $\beta x^2 \dot{x}$ , a source of energy for self-excitation  $\alpha \dot{x}$ , and a periodic driving at a frequency  $f_{\text{dr}}$ . This van der Pol oscillator can exhibit synchronization not only at  $f_{\text{dr}}/f_0 \approx 1$ , which is called harmonic synchronization, but at ratios that are rational numbers. If  $f_{\text{dr}}/f_0 > 1$ , the synchronization is said to be “superharmonic,” whereas if  $f_{\text{dr}}/f_0 < 1$  it is “subharmonic.”

For plasma waves, the van der Pol oscillator has been used both as a quantitative model and as a qualitative reference for the characteristic properties of synchronization. As a quantitative model, Eq. (1) has a limited usefulness because its nonlinear term does not exactly correspond to the nonlinearities in most kinds of plasma waves. Moreover, unlike a wave equation, Eq. (1) is a differential equation only

\*suranga-ruhunusiri@uiowa.edu

in time, not in position. For these reasons, in many cases the van der Pol oscillator is often best suited only as a *qualitative model*, which we will refer to in this paper as the *van der Pol paradigm*. In other cases, where the nonlinearity happens to take the same form as in Eq. (1), it can be used quantitatively, as has been suggested theoretically for ion sound waves that are self-excited by ionization [57], ionization waves self-excited by fluctuations in electron temperature [59], and oscillations in a beam plasma system [72].

The study of synchronization that we report in this paper is motivated by previous experiments of self-excited dust density waves, in the laboratory [30,38,39,54] and in microgravity conditions [46]. Using a sinusoidal driving voltage, Trottenberg *et al.* [30] observed harmonic synchronization and a narrower frequency spectrum, and later Pilch *et al.* [38,54] also observed subharmonic and superharmonic synchronization. Even without an external sinusoidal driving, some qualities of synchronization have been observed in microgravity experiments [46]. Synchronization played a role in earlier experiments with this wave as well; for example, in measurements of dispersion relations, the wave's frequency was determined by an externally applied modulation [18,32,33,41].

To characterize the synchronization of self-excited dust density waves, we carry out two experiments with a sinusoidal voltage applied to an electrode that is separate from the electrodes that sustain the plasma. We vary the driving frequency and driving amplitude, allowing us to determine the conditions that result in synchronization and to identify the mechanism for synchronization. We also observe a nonsynchronized oscillation, which we term a “nonharmonic state,” at a frequency that is well below both the natural oscillation frequency and the driving frequency.

The experiments and analysis are discussed in Sec. II. We present and interpret the results in Sec. III.

## II. EXPERIMENTS AND ANALYSIS

### A. Dusty plasma

Two experiments are performed under nearly identical conditions, one for making Arnold tongue diagrams and the other for identifying synchronization mechanism. The only difference between these two experiments is the method used for scanning the driving frequency and amplitudes as discussed in Sec. II C.

We prepare a plasma that has a dc electric field that can levitate dust particles against the downward force of gravity in a plasma sheath. The plasma is formed in a vacuum chamber (Fig. 1) with argon gas at 120 mTorr. A low power radio-frequency (rf) voltage, with a 57 V peak-to-peak amplitude is applied between two electrodes, one which is a horizontal lower electrode and the other which is the grounded wall of the vacuum chamber. This rf voltage produces an rf electric field that sustains the plasma by accelerating electrons that can partially ionize the gas. The 13.56 MHz frequency is so high that only electrons respond to it. In addition to the rf electric fields, there is also a dc electric field that arises naturally due to ambipolar transport of electrons and ions. In the sheath, immediately above the lower electrode, this dc electric field is mostly downward with a smaller horizontal component, and there is a significant ion flow in the direction of this dc electric field.

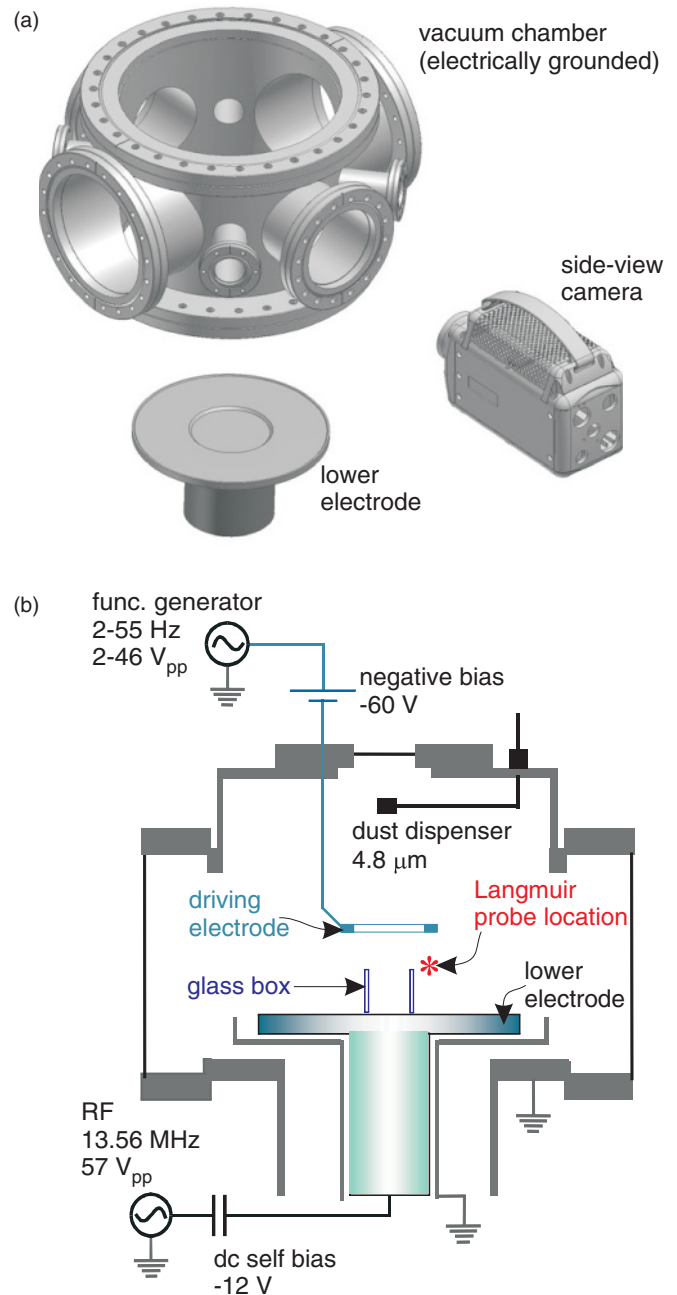


FIG. 1. (Color online) (a) Schematic of the vacuum chamber, shown without flanges. The high-speed camera is used for imaging the dust cloud. The lower electrode is inserted into the chamber during experiments. (b) Electrical and mechanical configuration. The 13 MHz rf oscillator is used to generate the plasma. By shaking a dispenser, we introduce dust particles so that they fall through the plasma. They collect a negative charge and become levitated and confined in a 3D cloud inside a glass box resting on the lower electrode. The plasma ion density is modulated by a ring-shaped driving electrode powered by a sinusoidal voltage, with an amplitude  $A_{dr}$  and a frequency  $f_{dr}$ . A Langmuir probe at a location outside the dust cloud, as marked \* is used to measure the ion density fluctuation due to driving. This probe is removed prior to adding dust. A photograph can be viewed in the Supplemental Material [78]. Note that the rf voltage and the driving voltage values are specified in peak-to-peak volts ( $V_{pp}$ ).

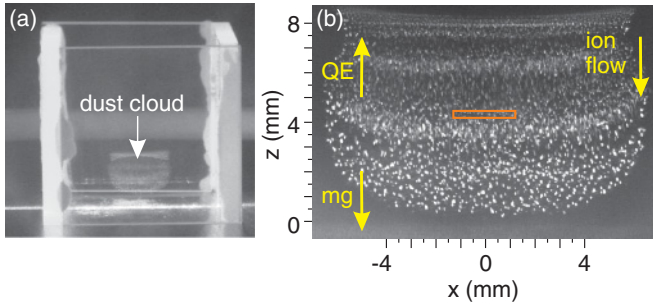


FIG. 2. (Color online) Side-view images of the dust cloud (a) showing its position inside the glass box (b) as recorded by the high-speed camera in Fig. 1. Charged dust particles are levitated by the upward electric force,  $QE$ , in balance with the downward gravitational force,  $mg$ . Self-excited dust density waves, which propagate downward, are visible as compressions and rarefactions. A measure of dust number density is obtained by averaging the image brightness within the sample region indicated by the rectangle. A movie that shows the propagation of self-excited dust density waves in the dust cloud is available in the Supplemental Material [78].

Dust particles, which are monodisperse melamine formaldehyde microspheres of diameter  $4.83 \mu\text{m}$ , are introduced into the plasma with a dust dispenser that is similar to a salt shaker with a single hole. Once they are immersed in the plasma, the dust particles acquire a negative charge. In the presence of the downward dc electric field, they experience an upward electric force that can balance the downward force of gravity, so that the dust particles are levitated (Fig. 2). To confine the dust particles in the horizontal direction, we enhance the horizontal component of the dc electric field by placing a glass box on the lower electrode, as in previous experiments [42,43,76,77]. The box has an open top, and its dimensions are  $3 \times 3 \times 3 \text{ cm}$ . A three-dimensional dust cloud, with a size of about 1 cm, is confined in the center of this box. We control the number of particles introduced so that in both experiments the dust cloud fills the same volume.

The wave fronts are easily visible in the images [Fig. 2(b)]. Bright and dark regions correspond to compressions and rarefactions of the wave, with a wavelength of about 2.5 mm. A movie can be viewed by online readers; see Ref. [78]. The waves propagate in the direction of the ion flow. The waves also grow in amplitude as they propagate because the energy gain from the ion-driven instability exceeds the dissipation due to frictional drag on the neutral gas atoms. We chose a gas pressure of 120 mTorr so that the frictional drag would be small enough to allow the waves to grow to nonlinear amplitudes after traversing only one-sixth of the cloud’s height.

The natural frequency of the dust density waves, i.e., the frequency in the absence of any periodic driving, is  $f_0 = 22$  and 21 Hz in the first and second experiments, respectively. We determined these frequencies not only by viewing the video but also by using the spectral analysis methods described in Sec. III A.

**B. Illumination and image capture**

The dust cloud is illuminated by a vertical sheet of 577-nm laser light, and it is imaged from the side with a digital camera

[Fig. 1(a)]. The illumination power of 0.9 W is low enough that it did not visibly perturb the dust cloud.

The camera records images at a rate of 256 frames per second, which is chosen to provide an adequate temporal resolution for the waves and their harmonics. The camera, with a 105-mm focal length lens and a doubler, provides a spatial resolution of 78 pixels/mm. At this resolution, a typical wavelength of 2.5 mm is resolved with about 200 pixels. The camera’s field of view includes the entire cross-section of the dust cloud that is illuminated, as shown in Fig. 2(b). In the image, a single particle spreads over about 25 pixels.

**C. External driving**

The self-excited dust density waves are altered by applying an external sinusoidal disturbance at a chosen frequency  $f_{\text{dr}}$  and amplitude  $A_{\text{dr}}$ . To do this, we disturb the overall ion density in the plasma by applying sinusoidal voltages to a negatively biased electrode located 2 cm above the top of the glass box [Fig. 1(b)]. This “driving electrode” is a flat copper ring with a surface area of  $15 \text{ cm}^2$ .

The external driving modulates the overall ion density in the chamber. We verify in a test that the sinusoidal ion density modulation varies linearly with the amplitude of the sinusoidal driving voltage at the same frequency. This linearity, shown in Fig. 3, extends over the entire range of driving amplitudes used in the experiments, including the lowest

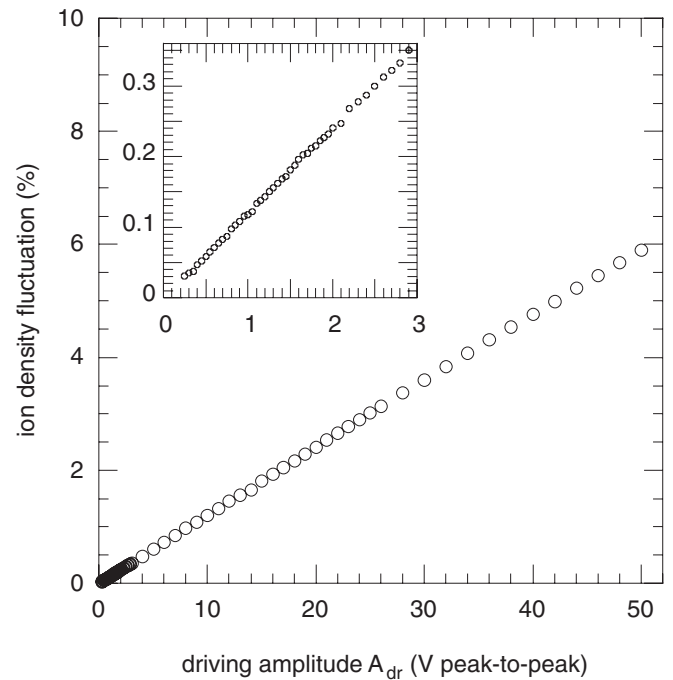


FIG. 3. Test of linearity in the response of the plasma to the driving. We measure the ion saturation current drawn by a negatively biased Langmuir probe, as a proxy for the ion density, at a location shown in Fig. 1. While applying a sinusoidal waveform at  $f_{\text{dr}} = 20 \text{ Hz}$  to the driving electrode, we measure the fluctuation in ion density, at that same frequency, using a lock-in amplifier. The inset is a magnification for the lowest driving amplitudes. This test demonstrates a linear plasma response to the driving over the entire range of driving amplitudes used in our experiments.

driving amplitudes, so that we are confident that the wave observations we will interpret as signatures of synchronization are not instead artifacts of a nonlinear response of the plasma to the driving. This linearity test is performed using lock-in-amplifier detection of current in a Langmuir probe biased for ion saturation.

Because harmonics can play an important role in nonlinear synchronization, we also verify that there is no detectable harmonic content in the ion density modulation. This test, which is also performed using our Langmuir probe, gives us confidence in our observations of harmonic content in dust density waves. These observations, presented in Sec. III, are not merely due to any harmonics present outside the dust cloud, but instead due to the more interesting physics of nonlinearities in the dust cloud.

The ion density modulation has the effect of modulating the Debye length and, therefore, the thickness of the sheath above the lower electrode [79]. Since the dust cloud is levitated by the dc electric field in this sheath, the small modulation of the ion density leads to a vertical shaking of the entire dust cloud, with a maximum displacement of  $\approx 1$  mm, as measured at  $f_{\text{dr}} \ll 20$  Hz and  $A_{\text{dr}} = 46$  V<sub>pp</sub>. Thus, our external modulation can affect the dust cloud in more than one way: a modulated ion density, a modulated dc electric field, and a resulting vertical shaking. We cannot identify which of these is responsible for the synchronization that we will observe.

We vary the driving frequency from 2 to 55 Hz. The upper limit of this range is chosen because we found in a test no signatures of synchronization at higher frequencies. Our two experiments differ in the procedures used for scanning the frequency  $f_{\text{dr}}$  and amplitude  $A_{\text{dr}}$ . In the first experiment, we slowly sweep the frequency, while in the second we hold the frequency constant. In both experiments the driving amplitude is held steady during the recording of a movie, and movies are repeated for various amplitudes starting with 2 V<sub>pp</sub>.

In our *first experiment*, we sweep the frequency, which allows us to measure wave conditions over many values of the driving parameters,  $A_{\text{dr}}$  and  $f_{\text{dr}}$ . These two parameters will be the axes of the Arnold tongue diagram that we discuss in Sec. III C, so that it is necessary to record wave data for many values of these two parameters in order to populate the diagram. Those data must be recorded for many values of  $A_{\text{dr}}$  and  $f_{\text{dr}}$  rapidly enough so that the number of particles within the dust cloud does not vary significantly. If we operate over a longer time, we would encounter the difficulty that the number of dust particles would diminish with time, especially when large-amplitude driving is applied. These requirements led us to use the method of Brandt [80]: sweeping the frequency  $f_{\text{dr}}$  at a constant amplitude, for a succession of amplitudes. We record data for the highest amplitudes at the end, so that the low-amplitude data are not affected by a loss of dust particles. The frequency is swept at a steady rate, from 2 to 55 Hz, over 145 s. One movie is recorded during this sweep, with its first frame triggered at the start of the sweep.

In our *second experiment*, we hold the frequency constant, so that the system is in a steady state during the recording of a time series. We rely on this second experiment for two purposes: to verify the validity of the results from the first experiment and to identify the synchronization mechanism. For the mechanism identification, we use the method of

Balanov [56], who held the frequency  $f_{\text{dr}}$  constant and then repeated for a series of driving amplitudes  $A_{\text{dr}}$ . Since this method of holding the frequency constant does not allow us to make observations over a wide a range of parameters, as does the sweeping method in the first experiment, in this second experiment we record data primarily for lower values of driving amplitudes, as is needed to identify the synchronization mechanism.

#### D. Image analysis

While in some dusty plasma experiments the positions of individual particles are measured from images, in this paper our analysis centers on a smoothed quantity, the dust number density  $n_d$ . In particular, we will determine the spectra of fluctuations of  $n_d$ . We can characterize  $n_d$  using images of the dust cloud because the camera's sensor has a linear response to incident light, and very little scattered laser light is absorbed within the dust cloud. To obtain the spectra of the fluctuations of  $n_d$ , we Fourier transform the time series of the brightness. In particular, we use the brightness averaged over a thin rectangular sample region in the image, indicated by a box in Fig. 2(b). This sample region is chosen to be only 0.25 mm in the  $z$  direction, i.e., about one-tenth of a wavelength in the direction of wave propagation, but a much wider 2.5-mm range in the  $x$  direction. We are able to average over such a wide range of  $x$  because the wavefronts are nearly planar in the center of the dust cloud.

### III. RESULTS

#### A. Time series and spectra of $n_d$

Examples of the time series of dust number density  $n_d$  are shown in Figs. 4(a) and 4(b), for two different driving frequencies  $f_{\text{dr}}$ , but the same large driving amplitude  $A_{\text{dr}} = 46$  V<sub>pp</sub>, as obtained from our first experiment. In Figs. 4(a) and 4(b), the fluctuation of dust number density is large, with a peak-to-peak fluctuation of about 50%, as compared to the time-averaged dust number density.

We calculate a spectrum of dust number density fluctuations from an interval within the time series. This is done by subtracting the time average and using a fast Fourier transform (FFT). We denote the frequency variable for this FFT, i.e., the spectral frequency, as  $f_{\text{sp}}$ , to avoid confusion with the driving frequency,  $f_{\text{dr}}$ . Our time interval for computing an FFT has a duration of 2 s, consisting of 512 frames. This duration is chosen to be short enough so that  $f_{\text{dr}}$  can be considered as a constant during that interval, but long enough so that the corresponding frequency resolution of 0.5 Hz allows us to distinguish the various synchronized states. Example spectra are shown in Figs. 4(c) and 4(d), computed for the time series data when the slowly swept  $f_{\text{dr}}$  was about 20 and 40 Hz, respectively.

We combine spectra for various driving frequencies, yielding Fig. 5(a). Such a graph of power as a function of the two frequencies,  $f_{\text{dr}}$  and  $f_{\text{sp}}$ , is useful for identifying synchronized states. The data in Fig. 5, as in Fig. 4, are for our highest driving amplitude,  $A_{\text{dr}} = 46$  V<sub>pp</sub>.

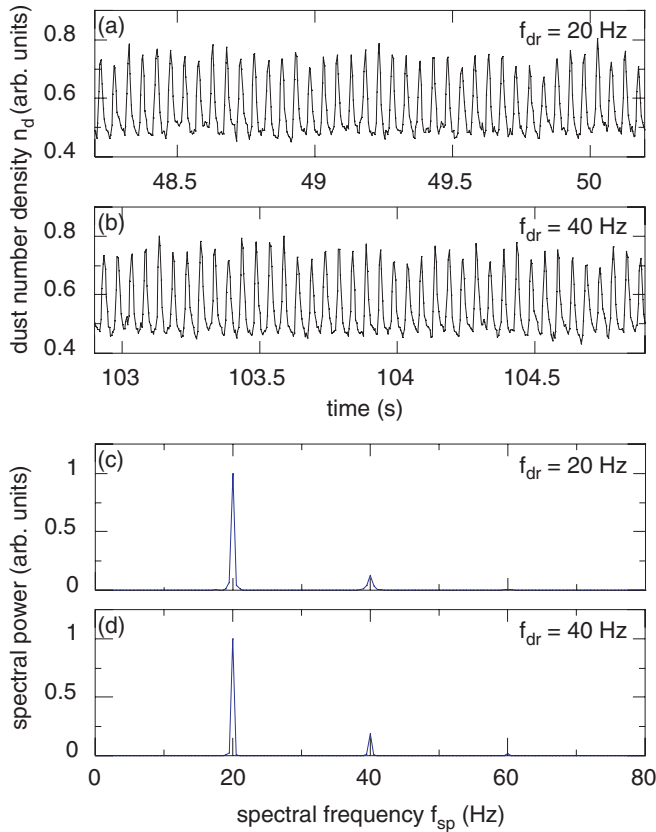


FIG. 4. (Color online) Brightness time series and spectra. Representative time series (a) and (b) of brightness, which is a measure of the dust number density  $n_d$ . The corresponding power spectra (c) and (d), calculated by fast Fourier transforming the fluctuations of  $n_d$ . The 2-s time interval used for the FFT is short enough that the slowly swept driving frequency  $f_{dr}$  can be considered to be constant. Two different synchronized states are shown: in (c) the observed wave at 20 Hz is synchronized to the 20 Hz driving frequency and a small harmonic is also present, while in (d) the wave at 20 Hz is synchronized to one half the 40 Hz driving frequency. These data from the first experiment are for  $A_{dr} = 46$  V<sub>pp</sub>.

## B. Features in the spectra

The spectra in Fig. 5 have a richness of detail, including three kinds of strong features that we will discuss, as well as some weaker features that we will not attempt to explain in this paper. The strong features are labeled in Fig. 5(b) according to our interpretation: the natural oscillation at  $f_0$ , synchronized states, and a nonharmonic state. We will discuss the natural oscillations and the synchronized states next. The nonharmonic state is a feature that is neither at  $f_0$  nor has signatures of synchronized states, and we will discuss it in Sec. III F.

### 1. Natural frequency

The natural frequency  $f_0$  can be identified as the dominant frequency in the spectrum *in the absence of driving*, i.e., at  $A_{dr} = 0$  V<sub>pp</sub>. Using data recorded without any driving, we were able to determine  $f_0 = 22$  Hz. This same natural frequency can also be present without, and even with, high-amplitude driving, provided that the driving frequency is either very low or high, as marked in Fig. 5(b).

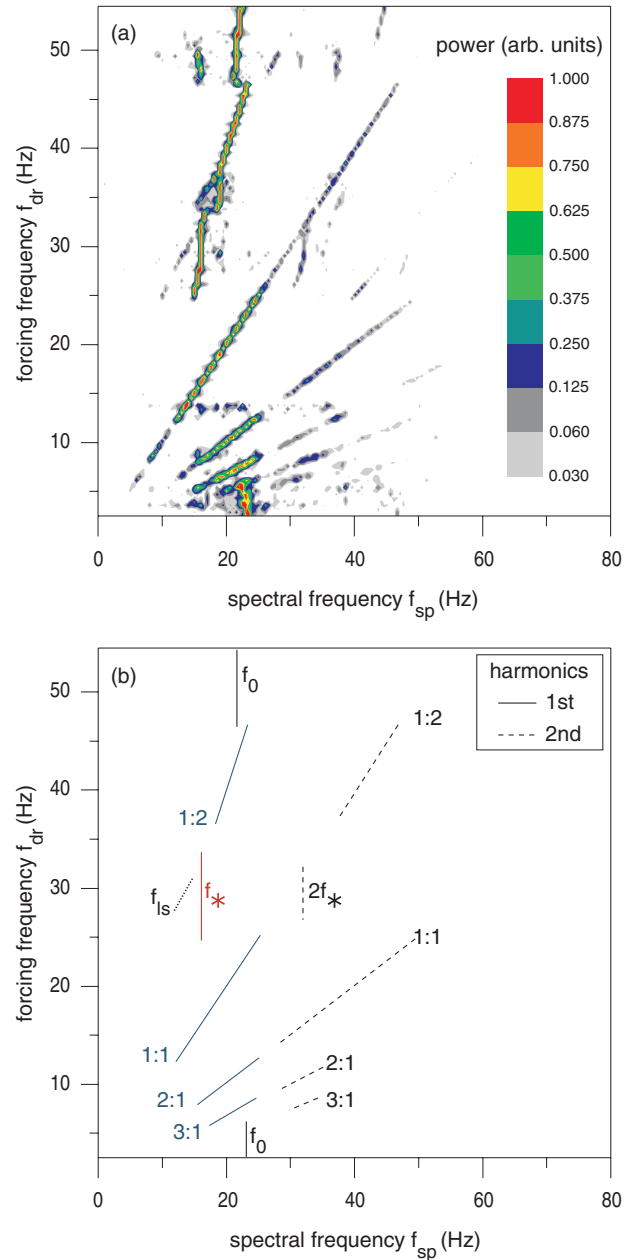


FIG. 5. (Color online) (a) Power spectra, as in Fig. 4, plotted with color representing power, for various driving frequencies. Data shown are from our first experiment for our highest driving amplitude,  $A_{dr} = 46$  V<sub>pp</sub>. Synchronized states, when they are present, are revealed by a line that extrapolates to the origin and has a constant slope, which is later referred to as the winding number. (b) Guide for interpreting the spectra in (a). At extremely low and high driving frequencies, oscillations are observed at the same natural frequency  $f_0$  as without any driving. Features of interest include: subharmonic 3:1 and 2:1 synchronization for  $5 < f_{dr} < 12$  Hz, harmonic 1:1 synchronization for  $12 < f_{dr} < 25$  Hz, and superharmonic 1:2 synchronization for  $35 < f_{dr} < 47$  Hz. The strongest spectral features are usually accompanied by their second harmonic, which is indicated by dashed lines in (b). Additionally, we observe a state marked  $f_*$ , termed the nonharmonic state in the text; it is neither a synchronized state nor an oscillation at the natural frequency,  $f_0$ . The presence of a lower sideband at a frequency  $f_{ls} \equiv f_{dr} - f_*$ , marked by a dotted line, and the presence of a second harmonic  $2f_*$  indicate that this state is nonlinear.

## 2. Synchronized states

At least four synchronized states are seen in Fig. 5. These appear as straight lines with an upward slope passing through the origin. The various synchronized states are distinguished by their slopes in Fig. 5. For example, the line marked 1:2 corresponds to oscillations at a frequency  $f_{sp}$  that is one half of the driving frequency,  $f_{dr}$ . This feature can be seen in the upper portion of Fig. 5. The 3:1, 2:1, 1:1, and 1:2 synchronized states are easily seen in Fig. 5. Synchronized states of 4:1 or higher may also be present, but their signatures at the bottom of Fig. 5 are too weak for us to identify them conclusively.

We now discuss the various synchronized states that we identify in Fig. 5. The synchronized state labeled 1:1 is termed the *harmonic* synchronized state. In this state, the external driving frequency  $f_{dr}$  is near, but not necessarily the same, as the natural frequency  $f_0$ , and the wave oscillates at the driving frequency  $f_{dr}$ . The synchronized states at an integer multiple of the driving frequency, labeled 2:1 and 3:1, are termed *subharmonic* synchronized states. In these states, the wave oscillates at a harmonic of the driving frequency. Finally, in the state 1:2, which is a *superharmonic* synchronized state, the wave oscillates at one half the frequency of the external driving.

All of these synchronized states are visible in Fig. 5 as a main spectral peak as well as peaks at integer multiples, i.e., at harmonics of the main peak. We have marked the second harmonics in Fig. 5(b) as dashed lines. Weaker features for third and higher harmonics can also be detected in Fig. 5(a). All these harmonics are present because the waves are non-sinusoidal, due to nonlinearities when the wave amplitudes are large [43]. We consider the peaks at the second- and higher-order harmonics as essentially part of the same synchronized state as the main peak, even though they can be distinguished in Fig. 5. For example, we consider the solid and dashed lines labeled 2:1 as both belonging to the same feature, which in this case is a subharmonic synchronized state.

Usually there is only one main peak for a given driving frequency,  $f_{dr}$ . The reader can confirm this by drawing a horizontal line across Fig. 5(a) and noting that this horizontal line intercepts only one peak with significant power, along with harmonics of that peak. For example, at  $f_{dr} = 20$  Hz, almost all the wave power is concentrated at  $f_{sp} = 20$  Hz, i.e., the 1:1 synchronized state.

Pilch *et al.* [38,54] have previously reported observing synchronization of dust density waves. They used a different kind of plasma source, an anode glow, which they modulated externally using the electrode that also sustains the plasma. Using video imaging similar to ours, they prepared time series of the brightness within spatially localized regions, analogous to our Figs. 4(a) and 4(b). From these time series, they computed frequency spectra, like our Figs. 4(c) and 4(d). By inspecting these spectra, they identified subharmonic, harmonic, and superharmonic synchronization.

### C. Arnold tongues

#### 1. Calculation method

We will next explore how the synchronization depends on the driving amplitude. This effort allows us to prepare a plot, known as an Arnold tongue diagram, which is a traditional characterization of nonlinear synchronization.

We will use data for the power as a function of frequency  $f_{sp}$  and driving frequency  $f_{dr}$ , as shown in Fig. 5(a). While the spectrum in Fig. 5(a) is prepared for only one driving amplitude, we also prepare similar spectra over a range of amplitudes. Altogether, these spectra represent power  $P$  recorded in a three-dimensional parameter space, with 120 values of spectral frequency  $f_{sp}$ , 105 values of driving frequency  $f_{dr}$ , and 29 values of driving amplitude  $A_{dr}$ .

An Arnold tongue is an indication, in the two-dimensional parameter space of driving amplitude versus driving frequency, of whether synchronization occurs. In our case, the parameter space for the Arnold tongue consists of 105 values of  $f_{dr}$  multiplied by 29 values of  $A_{dr}$ , for a total of 3045 elements. For each of these elements, we must make a binary decision whether the synchronization occurs, and if it does occur, we will darken that element in the parameter space. In this manner we draw an Arnold tongue.

One step in this process of drawing an Arnold tongue is often not described by practitioners: the manner of making the binary decision of whether synchronization occurs, for a given element of parameter space. We choose a specific procedure, with a quantifiable criterion for making the decision, which we now describe. First, using spectra data as in Fig. 5(a), we plot Devil's staircases (Fig. 6). The vertical axis in a Devil's staircase is a so-called winding number [56], which is the ratio of  $f_{dr}$  to the peak frequency, while the horizontal axis is the driving frequency,  $f_{dr}$ . To understand what we mean by the peak frequency, consider a horizontal profile of Fig. 5(a); this will be a line graph similar to the spectrum shown in Fig. 4(c). This spectrum has a distinctive peak, and it is the frequency of this peak that is used in calculating the winding number. To gain greater precision in determining the peak frequency, instead of merely selecting the spectral frequency with the highest power, the peak frequency is calculated [56] as a weighted mean  $\bar{f}$ ,

$$\bar{f} = \frac{\sum f_{sp} P}{\sum P}. \quad (2)$$

Here,  $P$  is the spectral power as a function of  $f_{sp}$ , as in Figs. 4(c) and 4(d). In using Eq. (2), we use values of the spectral frequency in the range  $0.5 \leq f_{sp} \leq 30$  Hz.

We now inspect the resulting Devil's staircase for a specific value of the driving amplitude, as in Fig. 6, and identify flat spots as a signature of synchronization. A quantifiable criterion is needed to decide whether a data point in the Devil's staircase is part of a flat spot. We make this decision by requiring that the winding number for the data point must be within 2% of the value of the data point to its left as well as within 2% of the data point to its right.

We now generate a graph of the Arnold tongues by repeating this decision for all 105 values of  $f_{dr}$  and all 29 values of  $A_{dr}$ , for a total of 3045 elements of the graph. Darkening an element when it was determined that it belonged to a flat spot in the Devil's staircase, we obtain the desired graph of Arnold tongues (Fig. 7). We use this method of generating Arnold tongues because the parameter space for a tongue is marked using only quantitative criteria, without any subjective interpretation to draw a tongue's boundary.

Our Arnold tongue diagrams are based on data from our first experiment, in which we sweep the driving frequency  $f_{dr}$ . This

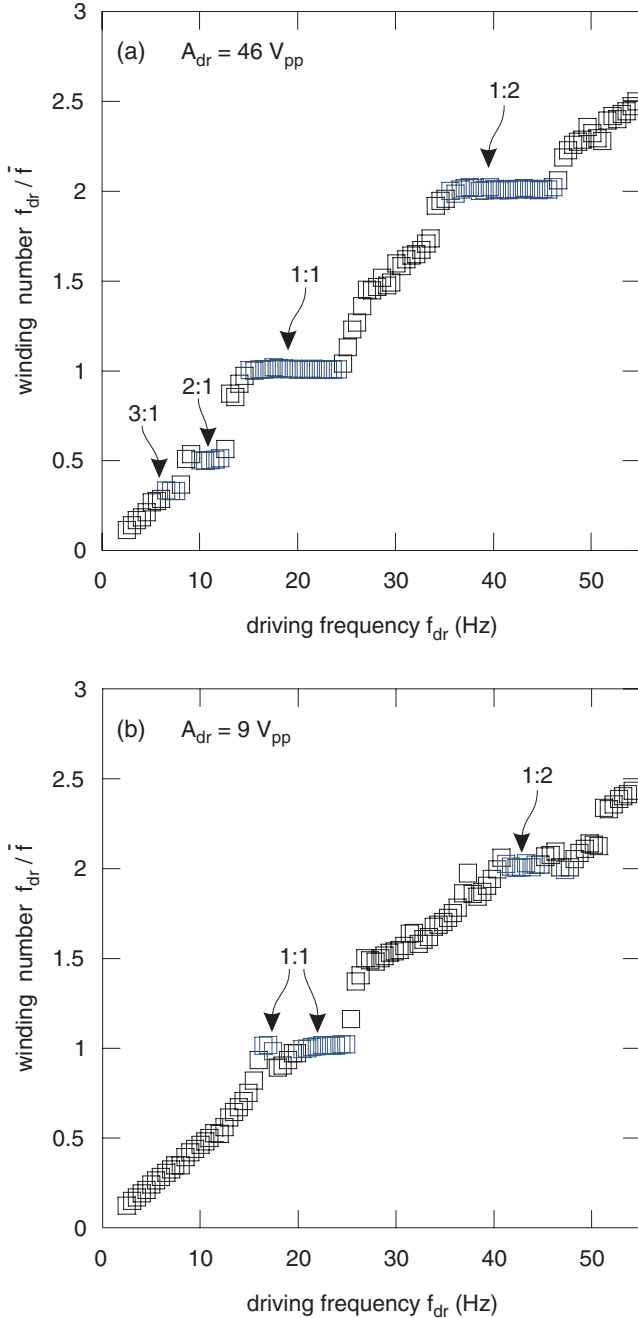


FIG. 6. (Color online) Devil's staircases, for measuring the range of driving frequencies for the synchronized states. (a) Data shown are from our first experiment for  $A_{dr} = 46 V_{pp}$ . This staircase plot is prepared using spectra as in Fig. 4 to calculate the frequency  $\bar{f}$  of the strongest peak, as in Eq. (2). The four flat spots indicated here correspond to harmonic 1:1, superharmonic 1:2, and subharmonic 3:1 and 2:1 synchronized states. Using a Devil's staircase like this one, we can measure the range of driving frequencies for each synchronized state; for example the 1:1 synchronized state at this driving amplitude occurs for  $14.5 \leq f_{dr} \leq 24$  Hz. (b) Data shown for  $A_{dr} = 9 V_{pp}$ . The two separate flat spots marked 1:1 indicate a branching of the 1:1 synchronized state, which will be shown in greater detail in Fig. 7.

sweeping allows us to cover a wide range of the parameters  $A_{dr}$  and  $f_{dr}$ , as is required for an Arnold tongue diagram, in a reasonable time before the dusty plasma conditions in the

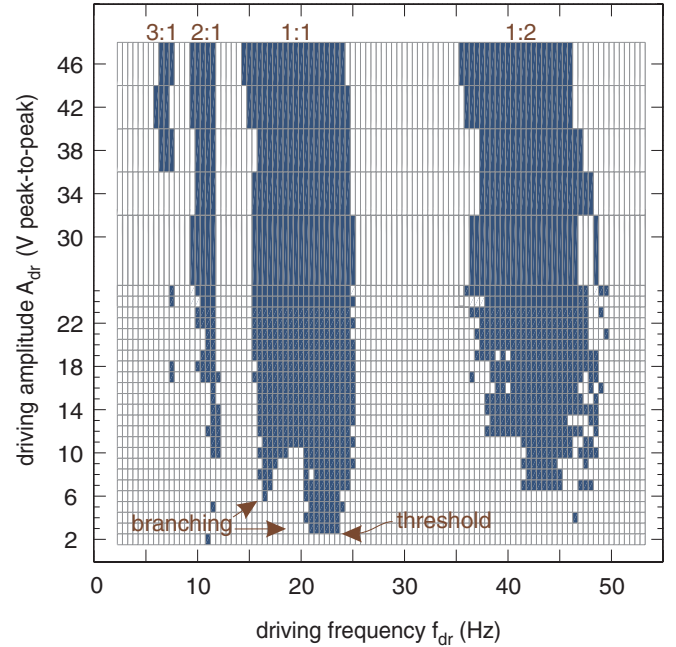


FIG. 7. (Color online) Arnold tongue diagram, i.e., indications of the driving conditions that result in synchronized states. Here we can identify four tongues for the harmonic 1:1, superharmonic 1:2, and subharmonic 3:1 and 2:1 synchronized states. To prepare this diagram, we marked the elements in the parameter space that correspond to a flat spot in the Devil's staircase in Fig. 6. Unlike Arnold tongues in the van der Pol paradigm, here the tongues do not narrow to a point at  $A_{dr} = 0 V_{pp}$ . Instead, we find a threshold driving amplitude for exciting synchronized states. Data shown are for our first experiment.

experiment changed. To verify that these results are unaffected by the use of sweeping, we checked the wave spectra in our second experiment and found that the peaks exhibited the signatures of synchronization as expected for the Arnold tongue diagram (Fig. 7).

## 2. Discussion of Arnold tongues

Our Arnold tongues in Fig. 7 reveal a *threshold* for the driving amplitude required for synchronization. Unlike the Arnold tongues for the van der Pol oscillator, ours do not have a sharp tip at zero driving amplitude but instead vanish at a small but finite amplitude. For example, there is no synchronization observed for  $A_{dr}$  below a threshold of  $6 V_{pp}$  for the 1:2 superharmonic synchronized state.

In considering the origin of this threshold, we must determine whether it is the result of nonlinearities in the dust cloud that we wish to study or whether it is instead an uninteresting consequence of the coupling of our driving electrode to the dust-free plasma located between the electrode and the dust. We can dismiss the latter possibility by examining Fig. 3, which demonstrates a linear response of the ion density to the driving amplitude. This response exhibits no threshold or other peculiarities, even at the lowest driving amplitudes. Thus, we assume that the origin of the threshold must lie somewhere within the dust cloud.

Our 1:1 Arnold tongue also has a distinctive *branching* at low forcing amplitudes. These branches can be seen in Fig. 7.

The two branches are at spectral frequencies of about 16 and 22 Hz.

We consider two possible explanations for this branching feature: the branches are either all part of the same 1:1 synchronized state or they indicate a merging of two different synchronized states. To test these explanations requires a way of distinguishing synchronized states, and for this purpose our Devil's staircase is a better tool than the Arnold tongue diagram, which is prepared from the Devil's staircase. By examining the rich detail in the Devil's staircase in Fig. 6(b), we find a signature of 1:1 synchronization feature with two separate flat spots at the same  $A_{\text{dr}}$  as the two branches in the Arnold tongue diagram. This indicates that both branches are in fact part of the same 1:1 synchronized state. A feature in Arnold tongue diagrams similar to our branching feature can be seen in the results of van der Pol simulations, which is not all belonging to the 1:1 synchronized state but instead a merging of two distinct nearby states such as 3:2 and 1:1 [81]. We can exclude the latter possibility by noting that our Devil's staircase lacks any signature of 3:2 synchronization, which would appear at a winding number of 0.6 if it were present in our experiment. Thus, we conclude that the branches we observed are all part of the same 1:1 synchronized state.

Similar branching of an Arnold tongue can be seen in previously reported experimental data for other physical systems, including the 1:1 synchronization of ionization waves in a non-dusty-plasma experiment [59] and the 1:1 synchronization of ruby laser output [82]. We use the term "branching" and not "splitting" as in Ref. [82] because only the tip of our 1:1 Arnold tongue is divided, not the entire tongue as in some of the results of Ref. [82]. Although this 1:1 branching is visible in these previously reported Arnold tongues [59,82], we have not found any explanation of this phenomenon in the literature.

#### D. Phaselocking versus suppression mechanisms

We will next determine which of the two synchronization mechanisms, in the context of the van der Pol paradigm, is responsible for the synchronization that we have observed. We will use the terms "phaselocking" and "suppression" to distinguish these two mechanisms, as defined by Balanov *et al.* [56].

To avoid confusion, we should mention that "phaselocking" and "suppression" also have other meanings in the synchronization literature. Phaselocking is used by some authors as a synonym for synchronization itself, regardless of its underlying mechanism [71]. The term "suppression" is used sometimes as a synonym for "oscillation death" in the literature for the nonlinear dynamics of biological systems [55]. The meanings we use for "phaselocking" and "suppression" are not these, but instead the synchronization mechanisms, as defined in Ref. [56].

To distinguish suppression and phaselocking, we follow the prescription in Sec. 3.9 of Balanov *et al.* [56]. They provided a comprehensive review of the fundamental theories and they presented a discussion of the signatures of suppression and phaselocking that we will use. These prescriptions were developed for use with the van der Pol oscillator, and we will use them even though that oscillator is essentially a single

point and not an extended system that sustains a propagating wave, like ours. Previous investigators of synchronization of plasma waves [58,73] relied upon the van der Pol paradigm for other purposes; here we rely upon it for distinguishing the two mechanisms that are possible for the van der Pol oscillator, phaselocking, and suppression [83]. In the van der Pol paradigm, suppression occurs over a wide range of driving amplitudes, except for the lowest amplitudes, where phaselocking can occur [56].

We now summarize the prescription of Balanov *et al.* [56] for determining whether the suppression and phaselocking mechanisms are present. The data used are power spectra. In particular, one examines two peaks in the spectra, at  $f_{\text{dr}}$  and  $f_0$ . A signature of phaselocking is a *merging* of the two peaks as the driving amplitude increases, while a signature of suppression is that the two peaks *remain separate* [56]. Another signature of the suppression is a significant *reduction* of the height of the peak at  $f_0$ , as the driving amplitude is increased. It is particularly useful to inspect the power spectra at lower driving amplitudes, corresponding to the lower portion of an Arnold tongue, because it is for these conditions that phaselocking, if it occurs at all, should be identifiable.

We next examine our spectra for the signatures of suppression and phaselocking. The spectral data we use for this purpose (Fig. 8) are from our second experiment. In particular, the conditions we consider are low driving amplitudes,  $A_{\text{dr}} \leq 12 V_{\text{pp}}$ , at  $f_{\text{dr}} = 16$  and 18 Hz, which are the same conditions as at the lowest extremity of the 1:1 Arnold tongue. We have marked the peaks at  $f_{\text{dr}}$  and  $f_0$  with heavy arrows at the top of each panel of Fig. 8. We will give close attention to the separation between these peaks, as indicated by the separation between the heavy arrows.

We can exclude the possibility of the phaselocking mechanism by observing that the peaks at  $f_{\text{dr}}$  and  $f_0$  never merge. Examining a column in Fig. 8, for example, the left column, we see that the separation between the peaks remains nearly constant and does not merge, as the driving amplitude increases from the top panel to the bottom. Thus, the signature of phaselocking (a merging of the two peaks) is absent. This result is the same for both cases, for  $f_{\text{dr}} = 16$  and 18 Hz.

We do observe the signature for the suppression mechanism, as indicated not only by the absence of merging, but also a significant reduction in the height of the peak at  $f_0$  as the driving amplitude increases. This reduction can be seen by scanning the eye downward in the left column of Fig. 8, focusing on the peak at  $f_0$ . For example, the power is reduced by about a factor of three between Figs. 8(b) and 8(d), and by about a factor of five between Figs. 8(d) and 8(e). This result for the driving frequency of  $f_{\text{dr}} = 16$  Hz in the left column is also confirmed in the right column for  $f_{\text{dr}} = 18$  Hz. Thus, as one of our chief results, we find that the 1:1 synchronization occurs through the mechanism of suppression and not phaselocking [84].

Additionally, we note that the spectra in Fig. 8 exhibit *sidebands*. These sidebands are peaks at frequencies that are linear combinations of  $f_{\text{dr}}$  and  $f_0$  and their harmonics, for example,  $f_{\text{dr}} + f_0$ ,  $2f_0 - f_{\text{dr}}$ , and  $3f_0 - 2f_{\text{dr}}$ , as marked by thin arrows in Fig. 8. In general, the presence of sidebands is interpreted as an indication that *nonlinear coupling* between

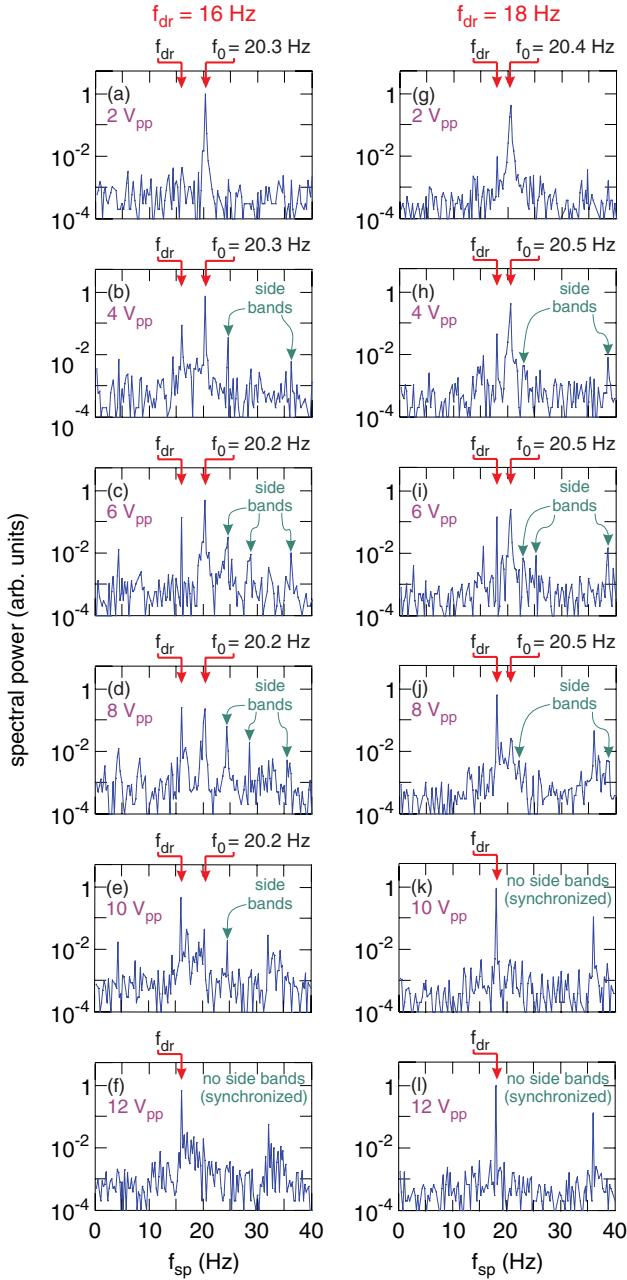


FIG. 8. (Color online) Testing for signatures of suppression vs. phaselocking mechanism, for 1:1 synchronization. We examine these spectra to identify how the peak for the natural frequency  $f_0$  behaves with respect to that of the driving,  $f_{dr}$ . (a) At the lowest driving amplitude, there is only a peak at the natural frequency  $f_0$ . (b)–(e) At a slightly higher driving amplitude, nonlinear coupling occurs, as indicated by the presence of sidebands, although the amplitude is not sufficient for synchronization. A transition to synchronization develops as the driving amplitude is increased (b)–(e), until the oscillation is fully synchronized with the driving in (f). In the transition to synchronization, we observe two indications of suppression: the two peaks do not merge, and the peak at  $f_0$  diminishes in height. Similar spectra are shown in the right column (g)–(l) and they exhibit the same signatures. These data are for the second experiment.

the waves and the external driving is present but too weak to result in synchronization [56].

### E. Period doubling and deterministic chaos

We also inspect our spectra for indications of chaos, and we find neither a signature of the periodic-doubling route to chaos nor any broadband spectral features that might indicate chaos. For the van der Pol oscillator, the period-doubling route to chaos can sometimes be observed at large driving amplitudes for driving frequencies that lie within the Arnold tongues. A signature of this transition is the appearance of subharmonic peaks at spectral frequencies of  $f_0/2^n$  [71]. Inspecting our spectra, we find no indication of these peaks, even for the highest driving amplitude that we used. We also find no indication of broadband spectral features, like the ones that have been reported for ionization waves, viz. Fig. 2(f) of Ref. [59]. Such broadband features sometimes occur when two Arnold tongues overlap, or inside the Arnold tongues [56,81], but we do not observe these broadband features. Thus, we conclude that we do not observe indications of dynamical chaos for the driving conditions that we used.

### F. Nonharmonic state

In the power spectra of Fig. 5, we noted three kinds of strong features, which we interpret as: the natural oscillations at  $f_0$ , the synchronized states, and a nonharmonic state that is neither synchronized nor at  $f_0$ . We now discuss this nonharmonic state, which is marked  $f_*$  in Fig. 5.

The feature  $f_*$  in Fig. 5 appears as almost a vertical line, meaning that the spectral frequency varies only a little while the driving frequency is varied over a wider range. In Fig. 5, the spectral frequency for this feature lies in the narrow range  $15 < f_{sp} < 17$  Hz, while the driving frequency has a wider range,  $25 < f_{dr} < 35$  Hz. We have verified that this feature is present in this same spectral frequency range for all driving amplitudes  $> 2 V_{pp}$  that we tested.

We term this feature as a “nonharmonic state,” since it appears to be different from both the natural oscillation at  $f_0$  and the synchronized states. The reason it appears not to be associated with the natural oscillation at  $f_0$  is that its spectral frequency is quite different, with  $f_*$  well below  $f_0$ . The reasons that we consider it not to be a synchronized state is that its frequencies do not match a subharmonic or superharmonic of the driving frequency  $f_{dr}$ , and it appears almost as a vertical line in the Fig. 5. This vertical line is unlike the synchronization features, which have constant slopes and pass through the origin.

We also find indications of nonlinearities for this nonharmonic state. These indications of nonlinearity are a harmonic at  $2f_*$ , as indicated by a dashed line in Fig. 5(b), and a lower sideband frequency,  $f_{ls} \equiv f_{dr} - f_*$ , as indicated by a dotted line in Fig. 5(b). The presence of this sideband indicates a nonlinear coupling of the external driving and the dust density waves. Thus, while we are unable to fully explain this feature, we can conclude that it is a nonlinear oscillation that is different from both the natural oscillation at  $f_0$  and the synchronized states. This nonharmonic state seems to occur above a threshold driving amplitude, since we do not observe it at our lowest driving amplitude of  $2 V_{pp}$ .

To further characterize the nonharmonic state, we determine the driving parameters for which it is observed from our first experiment, yielding Fig. 9. The uppermost portion of Fig. 9

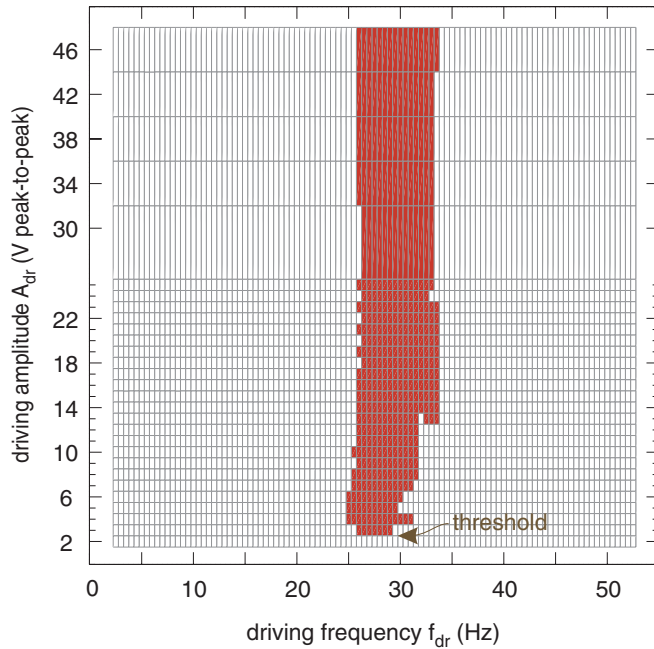


FIG. 9. (Color online) The driving parameter space for the condition we term the “nonharmonic state.” This diagram is prepared by examining spectra from our first experiment, like Fig. 5, for various driving amplitudes, and darkening an element in this parameter space if the strongest peak in the spectrum is between 15 and 17 Hz. Although this figure resembles an Arnold tongue diagram, it is different because Arnold tongue diagrams indicate the parameter space for synchronization, while this nonharmonic state is not synchronized.

corresponds to the largest driving amplitude, as in Fig. 5. In this plot of parameter space, we have darkened the portions corresponding to the nonharmonic state. This plot (Fig. 9) has a format similar to an Arnold tongue diagram, but we hasten to add that unlike an Arnold tongue, in this case the oscillations are not believed to be synchronized with the external driving at  $f_{dr}$ . A threshold for the driving amplitude required for this nonharmonic state is marked in Fig. 9. We verify the reliability of this observation of the nonharmonic state in our second experiment, with constant  $f_{dr}$ , by confirming that it is not an artifact of the sweeping.

#### IV. SUMMARY

We have characterized synchronization of the self-excited dust density waves in a dust cloud in a laboratory plasma. In the absence of driving, the waves propagate at a natural

frequency  $f_0$ . To provide driving, we apply a sinusoidal voltage with an adjustable driving frequency  $f_{dr}$  and driving amplitude  $A_{dr}$  to an electrode located above the dust cloud, causing the ion density throughout the plasma to be modulated sinusoidally at  $f_{dr}$ . As in the experiment of Ref. [43], the wave grows in amplitude as it propagates downward, attaining nonlinear amplitudes. We determine spectra for fluctuations in the brightness in video images, since the brightness is proportional to the dust number density. We examine how these spectra depend on the driving amplitude and frequency.

We find at least four distinct synchronized states: 3:1, 2:1, 1:1, and 1:2. In the harmonic synchronized state (1:1), the wave oscillates at the external driving frequency. For the subharmonic synchronized states (3:1 and 2:1), the wave oscillates at a harmonic of  $f_{dr}$ . We detect only one superharmonic synchronized state (1:2) in which the wave oscillations are at one-half the driving frequency.

Examining the spectra for the common signatures in the van der Pol paradigm, we find that synchronization of our waves has the signatures of the suppression mechanism but not the signature of the phaselocking mechanism. Additionally, we determined that period doubling and chaotic states were absent in our experiment.

The synchronization we observe differs in at least two additional ways from the van der Pol paradigm. First, there is a *threshold* that the driving amplitude must exceed for synchronization to occur, as can be seen in our Arnold tongue diagram (Fig. 7). Second, for 1:1 synchronization, our Arnold tongue does not have a single pointed tip, but instead has a *branched tip*.

We find that sidebands appear in the spectra at frequencies that are the sum or difference of  $f_0$  and  $f_{dr}$  or their harmonics. These sidebands are indications of nonlinear coupling. These are seen for driving conditions  $f_{dr}$  and  $A_{dr}$  that are slightly outside the Arnold tongues, i.e., for conditions that do not quite allow synchronization. These sidebands vanish for the synchronized states, as also occurs in the van der Pol paradigm.

We observe a feature in the spectra that we term a “nonharmonic state,” which appears to be a nonlinear oscillation. This feature appears in Fig. 5 at a spectral frequency between 15 and 17 Hz, which is neither the natural frequency nor a subharmonic or superharmonic of  $f_{dr}$ , as would be expected for a synchronized state. This nonharmonic state is not a familiar feature of the van der Pol paradigm.

#### ACKNOWLEDGMENTS

We thank M. Rosenberg and C. Brandt for helpful discussions. This work was supported by NSF and NASA.

- [1] D. A. Mendis and M. Rosenberg, *Annu. Rev. Astron. Astrophys.* **32**, 419 (1994).  
 [2] F. Verheest, *Space Sci. Rev.* **77**, 267 (1996).  
 [3] P. K. Shukla, *Plasma Phys. Control. Fusion* **42**, B213 (2000); *Phys. Plasmas* **8**, 1791 (2001).  
 [4] M. Rosenberg, *Astrophys. Space Sci.* **277**, 125 (2001).

- [5] A. Piel and A. Melzer, *Plasma Phys. Control. Fusion* **44**, R1 (2002); *Adv. Space Res.* **29**, 1255 (2002).  
 [6] D. A. Mendis, *Plasma Sources Sci. Technol.* **11**, A219 (2002).  
 [7] P. K. Shukla and A. A. Mamun, *Introduction to Dusty Plasma Physics* (Institute of Physics, Bristol, 2002).

- [8] P. K. Shukla and B. Eliasson, *Rev. Mod. Phys.* **81**, 25 (2009).
- [9] A. Melzer and J. Goree, in *Low Temperature Plasmas*, edited by R. Hippler, H. Kersten, M. Schmidt, and K. H. Schoenbach (Wiley, Weinheim, 2008).
- [10] O. Havnes, T. K. Aanesen, and F. Melandsø, *J. Geophys. Res.* **95**, 6581 (1990).
- [11] N. N. Rao, P. K. Shukla, and M. Y. Yu, *Planet. Space Sci.* **38**, 543 (1990).
- [12] A. Piel, *Plasma Physics: An Introduction to Laboratory, Space, and Fusion Plasmas* (Springer-Verlag, Berlin, 2010).
- [13] C. Thompson, A. Barkan, R. L. Merlino, and N. D'Angelo, *IEEE Trans. Plasma Sci.* **27**, 146 (1999).
- [14] J. H. Chu, J.-B. Du, and I. Lin, *J. Phys. D* **27**, 296 (1994).
- [15] N. D'Angelo, *J. Phys. D* **28**, 1009 (1995).
- [16] A. Barkan, R. L. Merlino, and N. D'Angelo, *Phys. Plasmas* **2**, 3563 (1995).
- [17] H. R. Prabhakara and V. L. Tanna, *Phys. Plasmas* **3**, 3176 (1996).
- [18] C. Thompson, A. Barkan, N. D'Angelo, and R. L. Merlino, *Phys. Plasmas* **4**, 2331 (1997).
- [19] R. L. Merlino, A. Barkan, C. Thompson, and N. D'Angelo, *Plasma Phys. Controlled Fusion* **39**, A421 (1997); *Phys. Plasmas* **42**, 1607 (1998).
- [20] E. Thomas Jr. and M. Watson, *Phys. Plasmas* **6**, 4111 (1999).
- [21] V. I. Molotkov, A. P. Nefedov, V. M. Torchinski, V. E. Fortov, and A. G. Khrapak, *J. Exp. Theor. Phys.* **89**, 477 (1999).
- [22] V. E. Fortov, A. G. Khrapak, S. A. Khrapak, V. I. Molotkov, A. P. Nefedov, O. F. Petrov, and V. M. Torchinsky, *Phys. Plasmas* **7**, 1374 (2000).
- [23] A. A. Samaryan, A. V. Chernyshev, O. F. Petrov, A. P. Nefedov, and V. E. Fortov, *J. Exp. Theor. Phys.* **92**, 454 (2001).
- [24] E. Thomas Jr. and R. L. Merlino, *IEEE Trans. Plasma Sci.* **29**, 152 (2001).
- [25] N. Hayashi, *Phys. Plasmas* **8**, 3051 (2001).
- [26] A. V. Zobnin, A. D. Usachev, O. F. Petrov, and V. E. Fortov, *J. Exp. Theor. Phys.* **95**, 429 (2002).
- [27] V. E. Fortov, A. D. Usachev, A. V. Zobnin, V. I. Molotkov, and O. F. Petrov, *Phys. Plasmas* **10**, 1199 (2003).
- [28] C. M. Ticoş, A. Dyson, P. W. Smith, and P. K. Shukla, *Plasma Phys. Controlled Fusion* **46**, B293 (2004).
- [29] M. Schwabe, M. Rubin-Zuzic, S. Zhdanov, H. M. Thomas, and G. E. Morfill, *Phys. Rev. Lett.* **99**, 095002 (2007).
- [30] T. Trottenberg, D. Block, and A. Piel, *Phys. Plasmas* **13**, 042105 (2006).
- [31] E. Thomas Jr., *Phys. Plasmas* **13**, 042107 (2006).
- [32] E. Thomas Jr., R. Fisher, and R. L. Merlino, *Phys. Plasmas* **14**, 123701 (2007).
- [33] J. D. Williams, E. Thomas Jr., and L. Marcus, *Phys. Plasmas* **15**, 043704 (2008).
- [34] C.-T. Liao, L.-W. Teng, C.-Y. Tsai, C.-W. Io, and I. Lin, *Phys. Rev. Lett.* **100**, 185004 (2008).
- [35] S.-H. Kim, J. R. Heinrich, and R. L. Merlino, *Phys. Plasmas* **15**, 090701 (2008).
- [36] L.-W. Teng, M.-C. Chang, Y.-P. Tseng, and I. Lin, *Phys. Rev. Lett.* **103**, 245005 (2009).
- [37] J. Heinrich, S.-H. Kim, and R. L. Merlino, *Phys. Rev. Lett.* **103**, 115002 (2009).
- [38] I. Pilch, T. Reichstein, and A. Piel, *Phys. Plasmas* **16**, 123709 (2009).
- [39] J. D. Williams and J. Duff, *Phys. Plasmas* **17**, 033702 (2010).
- [40] R. Fisher and E. Thomas Jr., *IEEE Trans. Plasma Sci.* **38**, 833 (2010).
- [41] E. Thomas Jr., *Phys. Plasmas* **17**, 043701 (2010).
- [42] T. M. Flanagan and J. Goree, *Phys. Plasmas* **17**, 123702 (2010).
- [43] T. M. Flanagan and J. Goree, *Phys. Plasmas* **18**, 013705 (2011).
- [44] A. Piel, M. Klindworth, O. Arp, A. Melzer, and M. Wolter, *Phys. Rev. Lett.* **97**, 205009 (2006).
- [45] A. Piel, O. Arp, M. Klindworth, and A. Melzer, *Phys. Rev. E* **77**, 026407 (2008).
- [46] K. O. Menzel, O. Arp, and A. Piel, *Phys. Rev. Lett.* **104**, 235002 (2010).
- [47] K. O. Menzel, O. Arp, and A. Piel, *Phys. Rev. E* **83**, 016402 (2011).
- [48] M. Rosenberg, *Planet. Space Sci.* **41**, 229 (1993); *J. Plasma Phys.* **67**, 235 (2002).
- [49] A. A. Mamun and P. K. Shukla, *Phys. Plasmas* **7**, 4412 (2000).
- [50] R. L. Merlino, *Phys. Plasmas* **16**, 124501 (2009).
- [51] F. Melandsø, T. K. Aslaksen, and O. Havnes, *J. Geophys. Res.* **98**, 13315 (1993).
- [52] F. Melandsø, T. K. Aslaksen, and O. Havnes, *Planet. Space Sci.* **41**, 321 (1993).
- [53] R. K. Varma, P. K. Shukla, and V. Krishan, *Phys. Rev. E* **47**, 3612 (1993).
- [54] I. Pilch, Ph.D. thesis, Christian-Albrechts-Universität, 2010.
- [55] A. Pikovsky, M. Rosenblum, and J. Kurths, *Synchronization: A Universal Concept in Nonlinear Sciences* (Cambridge University Press, Cambridge, 2001).
- [56] A. Balanov, N. Janson, D. Postnov, and O. Sosnovtseva, *Synchronization from Simple to Complex* (Springer-Verlag, Berlin, 2009).
- [57] B. E. Keen and W. H. W. Fletcher, *Phys. Rev. Lett.* **23**, 760 (1969); *J. Phys. D* **3**, 1868 (1970); *J. Phys. A* **5**, 152 (1972).
- [58] H. Amemiya, *Plasma Phys.* **25**, 735 (1983).
- [59] T. Klinger, A. Piel, F. Seddighi, and C. Wilke, *Phys. Lett. A* **182**, 312 (1993).
- [60] D. Block, A. Piel, C. Schröder, and T. Klinger, *Phys. Rev. E* **63**, 056401 (2001).
- [61] D. Block, C. Schröder, T. Klinger, and A. Piel, *Contrib. Plasma Phys.* **41**, 455 (2001).
- [62] C. Schröder, T. Klinger, D. Block, A. Piel, G. Bonhomme, and V. Naulin, *Phys. Rev. Lett.* **86**, 5711 (2001).
- [63] C. Schröder, T. Klinger, G. Bonhomme, D. Block, and A. Piel, *Contrib. Plasma Phys.* **41**, 461 (2001).
- [64] F. Brochard, G. Bonhomme, E. Gravier, S. Oldenbürger, and M. Philipp, *Phys. Plasmas* **13**, 052509 (2006).
- [65] C. Brandt, O. Grulke, and T. Klinger, *Plasma Phys. Controlled Fusion* **52**, 055009 (2010); *Phys. Plasmas* **17**, 032304 (2010).
- [66] M. E. Koepke, M. J. Alport, T. E. Sheridan, W. E. Amatucci, and J. J. Carroll III, *Geophys. Res. Lett.* **21**, 1011 (1994).
- [67] T. Klinger, F. Greiner, A. Rohde, A. Piel, and M. E. Koepke, *Phys. Rev. E* **52**, 4316 (1995).
- [68] T. Gyergyek, M. Čerček, N. Jelić, and M. Stanojević, *Phys. Lett. A* **176**, 54 (1993).
- [69] T. Gyergyek, M. Čerček, and M. Stanojević, *Contrib. Plasma Phys.* **37**, 399 (1997).
- [70] T. Gyergyek, *Plasma Phys. Controlled Fusion* **41**, 175 (1999).
- [71] T. Klinger, A. Piel, I. Axnäs, and S. Torvén, *Phys. Scr.* **56**, 70 (1997).
- [72] Y. Nakamura, *J. Phys. Soc. Jpn.* **28**, 1315 (1970).

- [73] Y. Saitou, Y. Nakamura, M. Tanaka, A. Komori, and Y. Kawai, *Plasma Phys. Controlled Fusion* **35**, 1755 (1993).
- [74] O. Fukumasa and R. Itatani, *Plasma Phys.* **24**, 1503 (1982).
- [75] B. van der Pol, *Philos. Mag.* **3**, 64 (1927).
- [76] O. Arp, D. Block, A. Piel, and A. Melzer, *Phys. Rev. Lett.* **93**, 165004 (2004).
- [77] O. Arp, D. Block, M. Klindworth, and A. Piel, *Phys. Plasmas* **12**, 122102 (2005).
- [78] See Supplemental Material at <http://link.aps.org/supplemental/10.1103/PhysRevE.85.046401> for a movie that shows downward propagating self-excited dust density waves and a photograph of the inside of the vacuum chamber.
- [79] T. E. Sheridan and J. Goree, *Phys. Fluids B* **3**, 2796 (1991).
- [80] C. Brandt, Ph.D. thesis, Ernst-Moritz-Arndt-Universität, 2009.
- [81] R. Mettin, U. Parlitz, and W. Lauterborn, *Int. J. Bifurcation Chaos* **3**, 1529 (1993).
- [82] J. Simonet, M. Warden, and E. Brun, *Phys. Rev. E* **50**, 3383 (1994).
- [83] In another example of using the van der Pol paradigm for a propagating wave, a chain of coupled van der Pol oscillators has been used as a model system to explain the periodic frequency pulling phenomenon they observed in the dust density waves [K. O. Menzel, O. Arp, and A. Piel, *Phys. Rev. E* **84**, 016405 (2011)].
- [84] We note that signatures of suppression have been reported for other plasma waves, for example, beam excited electron waves, viz. Fig. 3 of Ref. [74]. In a discharge current oscillation experiment, the obtained spectra, Fig. 12 of Ref. [67], seem to us to show signatures of phaselocking, although the authors did not remark upon them. Additionally, synchronization by suppression has been reported by other experimenters for ion acoustic waves (B. E. Keen and W. H. W. Fletcher, Ref. [57]), ionization waves (H. Amemiya, Ref. [58]), plasma relaxation oscillations (T. Gyergyek, M. Čerček, N. Jelić, and M. Stanojević, Ref. [68]), and beam plasma oscillations (Y. Nakamura, Ref. [72]; Y. Saitou, Y. Nakamura, M. Tanaka, A. Komori, and Y. Kawai, Ref. [73]), and the authors of these investigations did not mention synchronization by phaselocking.